ISSN 0937-9347, Volume 38, Number 4

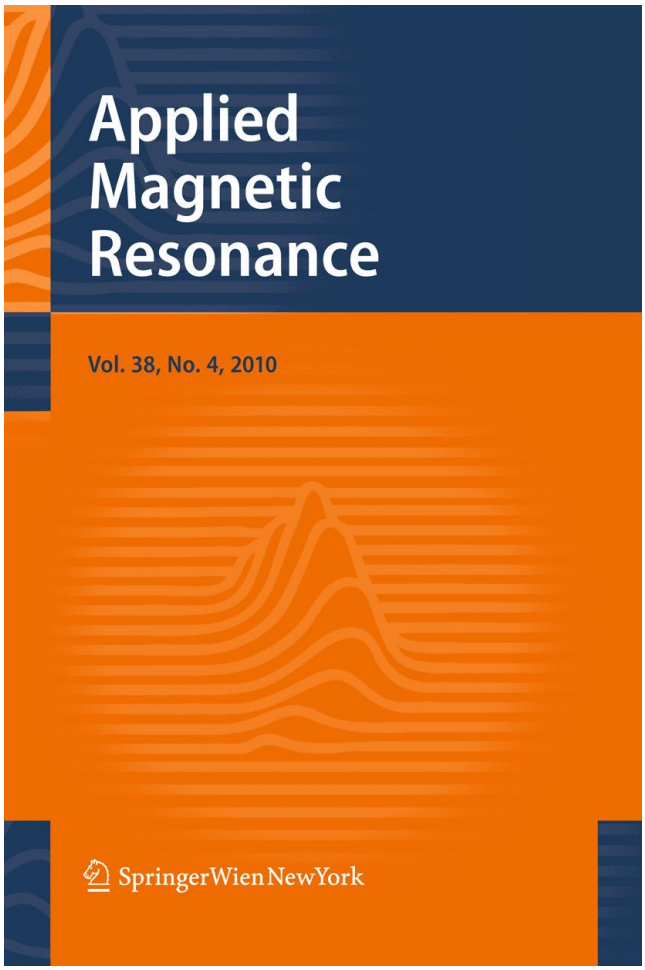

Appl Magn Reson (2010) 38:385–
DOI 10.1007/s00723-010-0120-5

Applied
Magnetic Resonance

EPR/FMR, FTIR, X-Ray and Raman Investigations of Fe-Doped SiCN Ceramics

S. I. Andronenko · I. Stiharu · D. Menard · C. Lacroix · Sushil K. Misra

Received: 6 December 2009 / Published online: 8 May 2010

Abstract SiCN magnetic ceramics doped with Fe ions were synthesized at different pyrolysis temperatures in the range from 600 to 1600°C. Several phases of ceramics were detected using the techniques of electron paramagnetic resonance/ferromagnetic resonance, Raman, Fourier-transform infrared and X-ray diffractometry, listed as follows: (a) transformation to the ceramic state from the polymer state, where the Fe ions are in the paramagnetic state, as the temperature is increased from 600 to 800°C; (b) formation of two different Fe species in the range of 950–1150°C: nanocrystalline particles in the ferromagnetic state and Fe ions incorporated into the free-carbon state in the superparamagnetic state; (c) diminution of the free-carbon content above 1150°C, and, as a consequence, diminution of the intensity of the broad Fe signal related to this phase; (d) appearance of a new Fe phase at about 1200°C; (e) disappearance of the ferromagnetic phase at about 1400°C; (f) disappearance of all Fe ions above 1530°C. The samples exhibiting superparamagnetic behavior are potentially useful in developing high-temperature magnetic sensor devices.

S. I. Andronenko · I. Stiharu
Department of Mechanical and Industrial Engineering, CONCAVE Research Centre, Concordia University, 1455 de Maisonneuve Boulevard West, Montreal, QC H3G 1M8, Canada

Present Address:
S. I. Andronenko
Physics Department, Kazan State University, Kremlevskaya 18, 420008 Kazan, Russian Federation

D. Menard · C. Lacroix
Département de génie physique, École Polytechnique de Montréal, C.P. 6079, succ. Centre-Ville, Montreal, QC H3C 3A7, Canada

S. K. Misra (✉)
Physics Department, Concordia University, 1455 de Maisonneuve Boulevard West, Montreal, QC H3G 1M8, Canada
e-mail: skmisra@alcor.concordia.ca

1 Introduction

In the last few years, a new ceramic material, polymer-derived SiCN (silicon carbonitride), has been exploited for microelectromechanical systems (MEMS) applications [1, 2]. Simple and effective manufacturing technologies for this material have been developed using liquid-polymer precursor technique [1, 2]. SiCN ceramics, derived from liquid polysilazane precursor, have many outstanding physical properties, such as hardness, fracture strength, creep resistance and high functional temperature. As well, these ceramics can be molded easily into complicated shapes characterized by very small dimensions. Magnetic Fe-doped SiCN ceramics, hereafter referred to as SiCN/Fe, can be easily produced by the addition of various iron-containing compounds to the polymer precursor. SiCN ceramics fabricated above 1000°C have excellent thermal and mechanical properties for high-temperature and high-pressure applications.

Superparamagnetic and ferromagnetic properties of magnetic SiCN/Fe ceramics can be used in building spintronic devices [3], functional at extremely high temperatures. Superparamagnetism occurs when the magnetic material consists of very small crystallites (1–10 nm). In a superparamagnet, the thermal energy is not sufficient at low temperatures to overcome the coupling between neighboring atomic paramagnets within a crystallite. In that case, the whole crystallite behaves as one magnetic dipole, characterized by a very large magnetic moment, which interacts with an applied magnetic field as a single dipole. The so-called "soft" magnets, based on SiCN nanostructured ceramic samples, possess very low coercivity with almost no magnetic hysteresis. Very large changes in the magnetic flux density within a superparamagnet are produced by the application of a rather small magnetic field, rendering them to be very sensitive magnetic sensors. In the ferromagnetic state, nanoparticles can exhibit ferromagnetic behavior, if their size is sufficiently large, wherein the internal crystalline part provides the possibility to produce ferromagnetic ordering of paramagnetic ions, exhibiting ferromagnetic resonance (FMR) lines. It is also possible to form a spin-glass state in amorphous materials with frustrated ferromagnetic exchange interactions between Fe ions.

SiCN ceramics, potentially useful for MEMS applications, have been extensively investigated in the past few years [1, 2, 4–20]. They consist of nanoparticles with an average size of 1.3 nm [4, 5, 9], which are formed at a pyrolysis temperature of as low as 1300°C as revealed by SAXS (small angle X-ray scattering) [5]. On the other hand, for the samples pyrolyzed at 1000°C, the presence of nanoparticles of carbon was confirmed by the relative intensity of D and G bands in Raman spectra [8]. This was not detected directly by transmission electron microscopy (TEM). This is because TEM imaging shows only homogeneous microstructure for such samples [9]. Furthermore, when the size of nanoparticles (carbon or SiCN) is in the order of 1 nm [5, 8], TEM cannot detect such particles, because their size is much less than the foil thickness illuminated by the electron beam. The existence of graphite nanoclusters of about 1 nm size in SiCN ceramics is quite possible, leading to the formation of superparamagnetic clusters of Fe, embedded in such graphite nanoparticles. The nanostructure of SiCN ceramics, including a free-carbon phase

and a SiCN ceramic network, plays a very important role in the magnetization of the SiCN/Fe material, as discussed below.

The free-carbon phase in SiCN ceramics forms the so-called "cage" structure [11, 12], proposed initially in the context of SiCO ceramics. Magnetic impurities, such as Fe ions, can be incorporated in the SiCN structure consisting of nanoparticles. Superparamagnetism then arises from the magnetic coupling of Fe magnetic moments inside the nanoparticles. Other Fe inclusions with larger size can exhibit ferromagnetic behavior. The superparamagnetic nature can be studied by electron paramagnetic resonance (EPR) spectroscopy.

Polymer-derived magnetic SiCN/Fe composites were first synthesized by Saha et al. [13] from CERASET^{TM} solution using Fe_2O_3 powder. In the final ceramic composite, particles of α-Fe, iron silicate (Fe_2SiO_4) and FeN were found. They limited the pyrolysis temperature to 1100°C. SiCN ceramics with the addition of ferrocene was synthesized by Dumitru et al. [14, 15]. Presence of Fe_3C and Fe_3C coated with carbon in the SiCN ceramics fabricated at the pyrolysis temperature of 1200°C, was detected by X-ray diffraction and magnetic moment measurements. Li et al. [16, 17] also reported preparation of SiCN/Fe magnetic ceramics from polysilazane. They synthesized SiCN/Fe ceramics at the rather low temperature of less than 1100°C and found low coercivity in their samples, which depended upon atmosphere and temperature of pyrolysis. Only α-Fe was found as a source of magnetism.

The EPR technique has been successfully used to investigate pure SiCN ceramic samples [6–8]. In particular, a detailed investigation of dangling bonds in these ceramics was carried out by EPR at several frequencies from 9.5 GHz to as high as 170 GHz at various temperatures from 4 to 300 K [6]. There was observed an intense EPR line due to carbon-related sp^2-dangling bonds [6], located on the surface of free-carbon phases with $g = 2.0027$. These dangling bonds were formed during ceramization, after which C–H bonds were broken, allowing for the formation of a free-carbon phase.

It is the purpose of this paper to report the results of a detailed EPR/FMR study on SiCN/Fe ceramics derived from liquid polyureasilazane precursor. This will provide detailed information on the nature of contributions from different sources of magnetism in these ceramics.

2 Synthesis of Fe-Doped SiCN Ceramics

The samples were prepared following the well-known process of fabrication of SiCN ceramics [1, 2], using liquid precursor CERASET^{TM} polyureasilazane, to which 5–10 wt% of iron(III) acetylacetonate was added because of its good dissolution in liquid CERASET^{TM}, which was mixed with 0.5 wt% of dicumyl peroxide to decrease thermosetting temperature to 160°C from the usual 220°C for pure CERASET^{TM}. It is noted that for Fe doping, the iron(0) pentacarbonyl $Fe(CO)_5$ was also used here. It is in the liquid state and dissolves better in CERASET^{TM}. The resulting SiCN/Fe ceramics pyrolyzed at 1100°C exhibited, in general, the same EPR/FMR lines, as did the ones prepared with Fe(III)

acetylacetonate. This solution was then stirred for 2 h, and filtered to remove undissolved particles of powder to obtain a transparent dark-red liquid. The solution was poured inside a mold and thermoset at 160°C for 60 min under flowing nitrogen gas. Thereafter, the samples were removed from the mold and cross-linked at 400°C for 90 min to produce transparent dark-red solid polymer. This bonded the polymer chains of polyureasilazane into the polymer network, wherein the hydrogen ions were detached from the nitrogen ions, which became incorporated into the polymer chains bonding them together. The cross-linked polymer was then pyrolyzed at chosen temperatures between 600 and 1600°C in the presence of nitrogen gas for 4 h with the heating rate of 4°C/min to yield solid ceramic samples. The pyrolysis eliminated excess carbon forming CH_4 molecules and precipitated free carbon, leading to incorporation of some carbon ions into the mixed tetrahedral Si–C–N structure. A Barnstead Thermolyne tube furnace F21135 with the maximum processing temperature of 1200°C was used for thermal treatments below 1150°C. On the other hand, a high-temperature, high-pressure furnace, manufactured by Thoughtventions Unlimited LLC, was used for thermal treatment above 1200°C. During pyrolysis, the heating/cooling rate was 4°C/min and the dwelling time was 4 h. The composition of polymer-derived ceramics, as determined by elementary chemical analysis, was found to be $SiC_{0.68}N_{0.41}$ at the pyrolysis temperature of 1100°C. At high pyrolysis temperatures, the content of N decreased to 0.15, accompanied by 30 wt% of carbon in the free-carbon phase. Increasing the pyrolysis temperature led to increased removal of H atoms and formation of dangling bonds on the periphery of the free-carbon phase, as suggested by Trassl et al. [7–9]. In addition, there were formed carbon-bonded dangling bonds in the body of SiCN ceramic network as defects. Finally, no oxygen was found to remain in the samples. Neutron-activated analysis of SiCN/Fe composite determines the value of Fe content to be 0.2 wt%.

3 EPR Results and Transformations at Various Pyrolysis Temperatures

A Bruker ER-200D SRC EPR X-band ($\sim$9.5 GHz) spectrometer equipped with Oxford helium-flow cryostat was used to investigate the SiCN/Fe ceramic samples in the temperature interval of 77–350 K. Figure 1 shows room temperature EPR spectra for the various samples pyrolyzed at different temperatures. The EPR signals observed in SiCN/Fe composites are due to Fe^{3+} ions incorporated into the SiCN network, free-carbon phase and ferromagnetic crystalline particles, in addition to the very narrow EPR signal due to carbon-related dangling bonds. Several transformations of SiCN/Fe ceramics were noted as deduced from the behavior of the various EPR lines that included the dependence of the width and double-integrated intensity of the first-derivative EPR line (area under the EPR absorption line) of the various Fe EPR lines on the pyrolysis temperature of the samples. The interpretation of the various EPR signals is as follows.

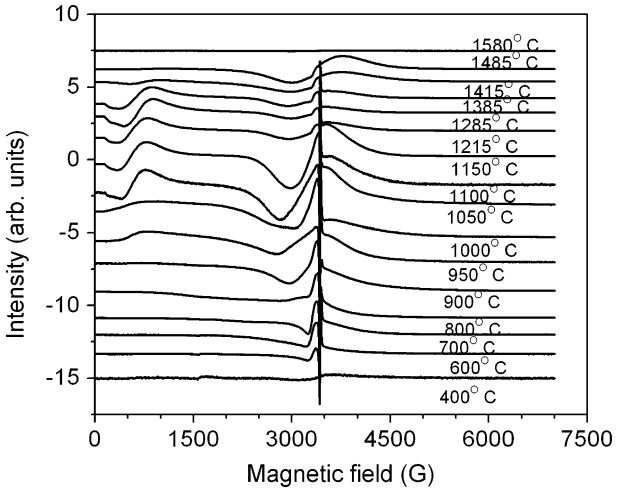

Fig. 1 Room temperature EPR spectra showing the dependence of Fe FMR/EPR spectra on the pyrolysis temperature

3.1 Narrow EPR Line due to Dangling Bonds at $g = 2.0027$

The double-integrated intensity of the first-derivative signal due to sp^2 carbon dangling bonds situated at $g = 2.0027$ is shown in Fig. 2. It exhibited the maximum for samples pyrolyzed at about 1000–1100°C. The dependence of the line width of this EPR signal on the pyrolysis temperature of the various samples is shown in Fig. 3, which demonstrates that with increasing pyrolysis temperature, the EPR line width decreases, achieving its minimum at about 1450°C. The peak-to-peak first-derivative EPR line widths due to dangling bonds in Fe-doped samples were found to be considerably larger (2.4 and 5.3 G for 1 and 10 wt% iron acetylacetonate, respectively) than that in pure SiCN ceramic samples (1.2 G), for SiCN/Fe samples pyrolyzed at 1100°C. This increase in width is due to the dipole–dipole interactions between carbon-related dangling bonds and Fe^{3+} ions. Above 1500°C, the intensity of the EPR line due to dangling bonds decreased, and the line became broadened due to crystallization of SiCN and disappearance of the free-carbon phase, which further reduced the number of dangling bonds.

3.2 Broad intense Fe^{3+} EPR Signals near $g \sim 2$

Two EPR lines were observed at room temperature. The dependence of the area under this absorption lines, which are the double integrals of this first-derivative EPR line, on the pyrolysis temperature is shown in Fig. 4, whereas the dependence of the peak-to-peak line width of the first-derivative EPR line on the pyrolysis temperature is shown in Fig. 5. For samples fabricated at pyrolysis temperatures of 950–1150°C, this line clearly consists of two broad lines (A and B) with different widths as shown in Fig. 4. The line width of the signal A changes significantly with

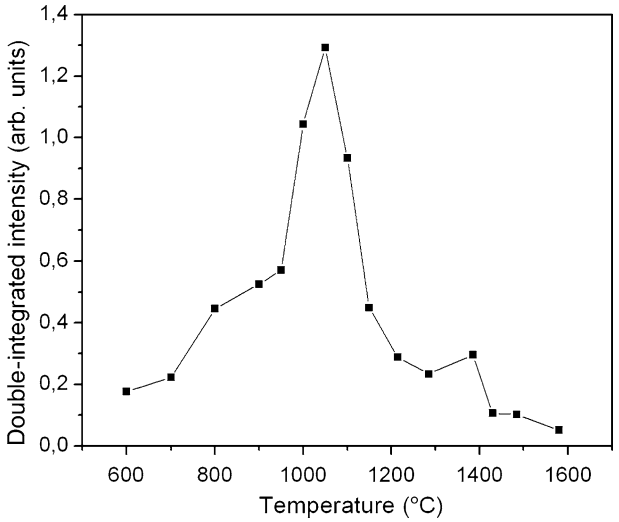

Fig. 2 Dependence of the double-integrated intensity of the first-derivative EPR signal of dangling bonds on the pyrolysis temperature of various samples

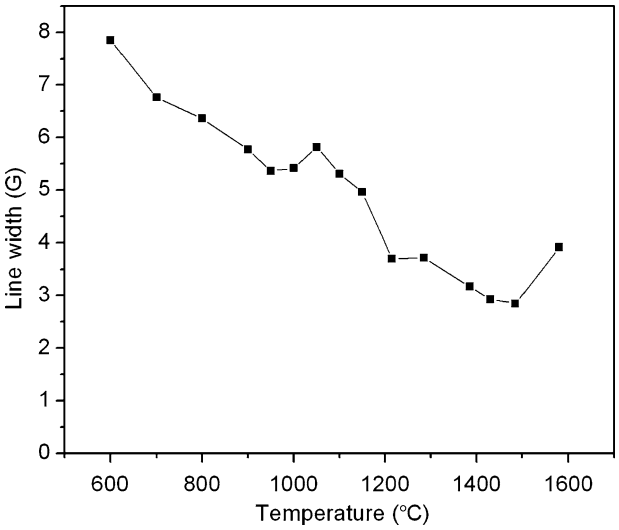

Fig. 3 Dependence of the EPR line width of dangling bonds on the pyrolysis temperature of various samples

temperature, exhibiting the maximum for the sample pyrolyzed at 1100°C, whereas the width of the associated signal B has increased only slowly. From these behaviors, it is deduced that the line A is due to the Fe^{3+} ions incorporated in the amorphous carbon phase, whereas the line B is due to the Fe^{3+} ions incorporated in the ordered carbon phase.

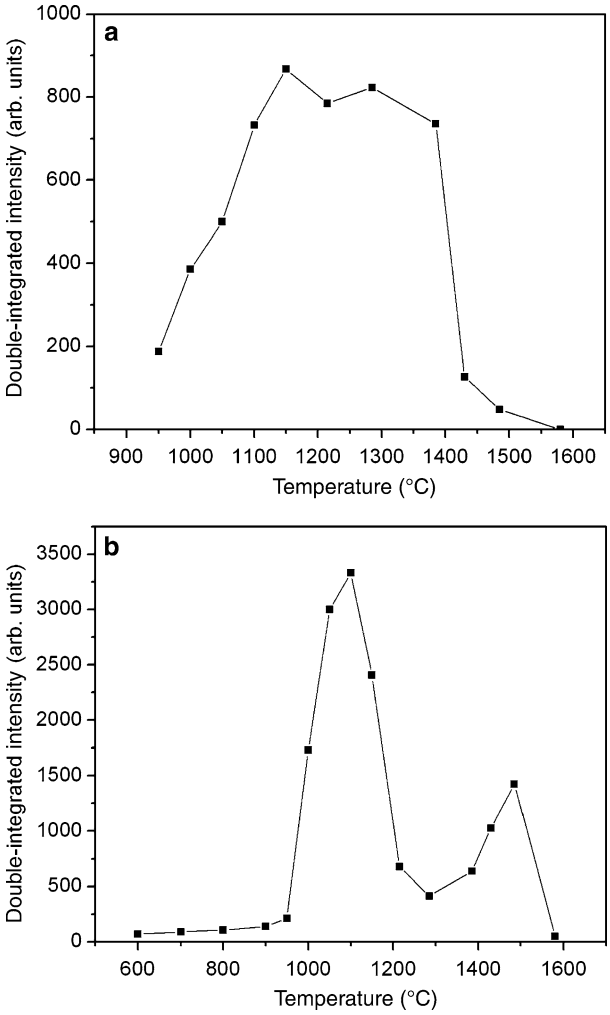

Fig. 4 Dependence of the double-integrated intensity of the Fe FMR/EPR signal on the pyrolysis temperature: **a** for the line at $g \sim 10$; **b** for the broad line at $g \sim 2.0$

From Figs. 4 and 5, it is seen that there is a correlation between the double-integrated intensity of the EPR signal of dangling bonds depending on the pyrolysis temperature and the double-integrated intensity of the Fe EPR signal that occurs at $g \sim 2.0$, whose intensity is proportional to the magnetic moment of the Fe ions, since the double-integrated signal of dangling bonds is proportional to the amount of the free-carbon phase in SiCN ceramics. This implies that the Fe ions are incorporated into the free-carbon phase. The features of the EPR signals from the various samples pyrolyzed at different temperatures can be summarized as follows:

(i) In the samples pyrolyzed at temperatures 600–800°C, where the SiCN structure is not yet completely formed, the Fe ions are in the paramagnetic state

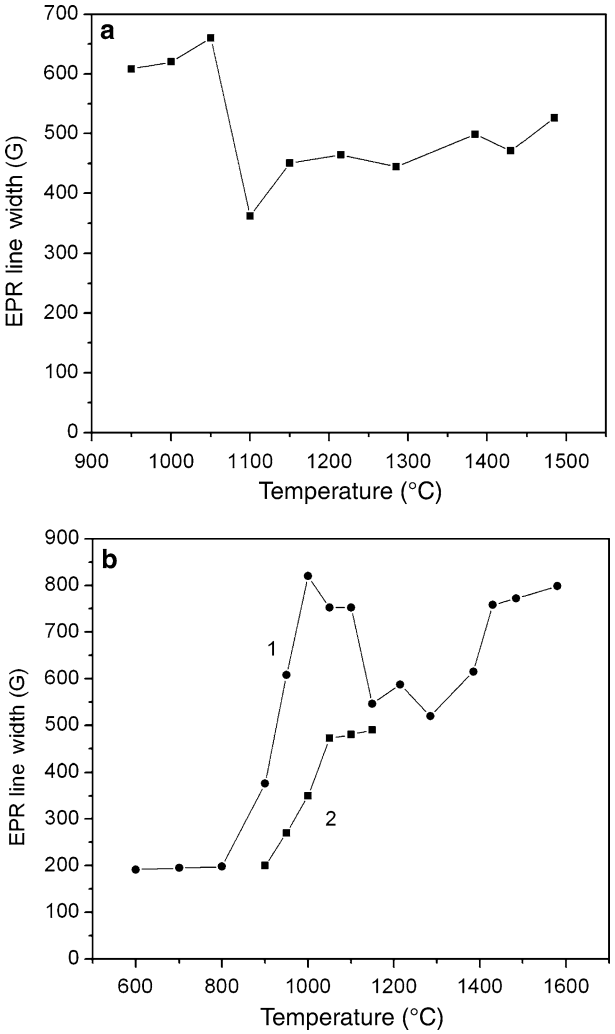

Fig. 5 Dependence of the Fe FMR/EPR line width at room temperature on the pyrolysis temperature: **a** for the line at $g \sim 10$; **b** for the broad line at $g \sim 2.0$ (*closed circles* and *closed squares* indicated the two *overlapped lines*)

possessing very small magnetization, as evidenced by the small value of the double-integrated EPR intensity. (ii) For the samples prepared at the pyrolysis temperatures of 800–1150°C, the double-integrated intensity of the first-derivative Fe EPR signal is very large, although the overall content of Fe atoms is still the same. This implies that the increase of the Fe magnetic moment is due to the formation of a nanosized structure of SiCN, which, in turn, is the nanosized structure of the free-carbon phase, wherein the Fe ions are in the superparamagnetic state with large magnetic moments. The existence of the superparamagnetic behavior is also supported by the results of Li et al. [16, 17], where the coercivity was found to be very low and

ranged from 50 to 463 G in SiCN/Fe ceramics pyrolyzed at different temperatures. (iii) The double-integrated intensity of the broad line at $g \sim 2.0$ decreased for the samples pyrolyzed above 1150°C. But at the same time the third narrow Fe line, situated at $g \sim 2$, appears, implying that a part of Fe ions transfer to a new magnetic structural state. (iv) The double-integrated intensity of the broad EPR line at $g \sim 2.0$ increased again for the samples prepared at the pyrolysis temperatures of 1400–1500°C as seen from Fig. 4b. This is due to the fact that the EPR line at $g \sim 10$ disappears at these temperatures and the Fe ions previously incorporated in the Fe_5Si_3 crystallites also contributed to the broad line at $g \sim 2.0$.

3.3 EPR Line at $g \sim 10.0$

This line is due to the formation of ferromagnetic crystallites incorporated into the SiCN ceramics, which form at the pyrolysis temperature of 950°C. It completely disappeared for the samples prepared at the pyrolysis temperature of 1430°C and above. Assuming here that the size of ferromagnetic crystallites in SiCN is considerably larger than that of the usual SiCN grains ($\sim$1.3 nm), crystallites exhibit ferromagnetism rather than superparamagnetism, since the latter requires a smaller size, on the order of that of grains of the SiCN (1.3 nm). As it will be shown below, it is most likely that these ferromagnetic crystallites are Fe_5Si_3 nanocrystallites, as deduced here from its low Curie temperature (T_C = 409 K).

3.4 Weak EPR Line at $g \sim 2.0$

This signal appears only in samples prepared at the pyrolysis temperatures above 1215°C, at which crystallization of the SiCN network starts. This signal is characterized by a narrow line width (100 G). It disappears completely in the samples prepared at the pyrolysis temperature larger than or equal to 1485°C. This signal can be ascribed to the Fe^{3+} ions incorporated in Si_3N_4 nanocrystallites, which start to crystallize at 1200°C, as shown by X-ray powder diffraction analysis.

3.5 Samples Pyrolyzed above 1500°C

No EPR lines due to Fe^{3+} ions are observed in these samples, because of evaporation of Fe ions from SiCN ceramics above 1530°C, the melting temperature of iron.

4 Temperature Dependences of Fe^{3+} EPR Lines

4.1 EPR Line at $g \sim 10$

The g value, double-integrated intensity of the first-derivative EPR signal, and the peak-to-peak line width of the EPR signal for the SiCN ceramic sample prepared at the pyrolysis temperature of 1100°C in the temperature range of 77–400 K are shown in Figs. 6, 7 and 8, respectively. It is seen that their temperature behavior is consistent

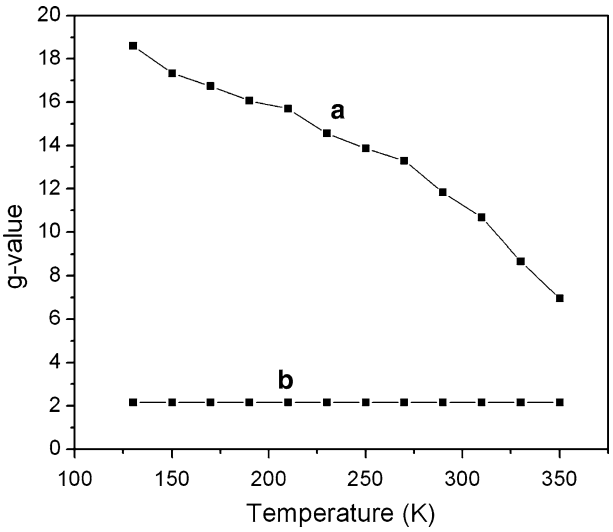

Fig. 6 Temperature dependence of the g value of the Fe FMR/EPR lines: *a* for the line at $g \sim 10$, *b* for the line at $g \sim 2.0$

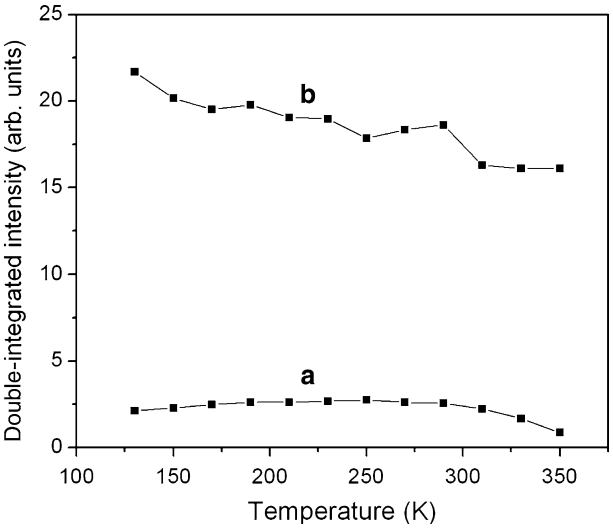

Fig. 7 Temperature dependence of the double-integrated intensity of the first-derivative FMR/EPR line: *a* for the line at $g \sim 10$; *b* for the line at $g \sim 2.0$

with the temperature dependence of the magnetic moment of the ferromagnetic Fe_5Si_3 particles characterized by the Curie temperature of 400 K. This is confirmed here by fitting, using the following expression for the temperature (T) dependence of the FMR line width of impurity centers in a ferromagnetic sample [21]:

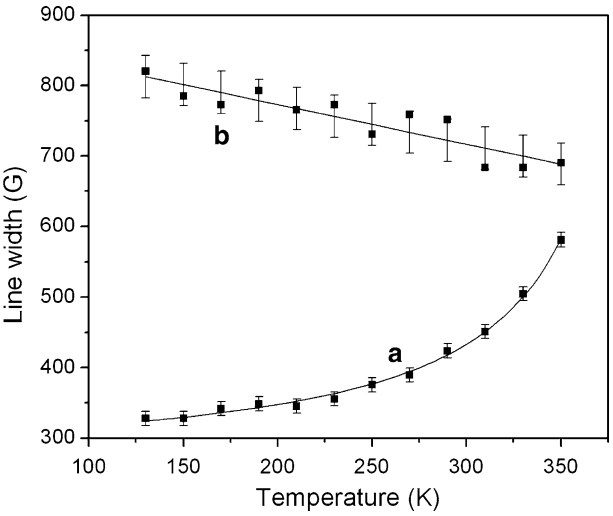

Fig. 8 Temperature dependence of the FMR/EPR line width: *a* for the line at $g \sim 10$; *b* for the line at $g \sim 2.0$. *Continuous lines* represent the results of simulations with parameters, listed in the text

$$\Delta B = \Delta B_0 + A|T_C - T|^{-0.7}. \quad (1)$$

The fit to Eq. (1) yielded the values $\Delta B_0 = (220 \pm 10)$ G, $A = (5.2 \pm 0.5) \times 10^3$ G·K$^{0.7}$, and $T_C = (393 \pm 5)$ K. It is noted that this Curie temperature is very close to $T_C = 393$ K for Fe_5Si_3 [22].

The line width expression described by Eq. (1) is justified as follows. A considerable contribution to the FMR line width in ferromagnetic samples comes from fluctuations of the magnetization M near the Curie temperature. Since the magnetization shifts the position of the resonance, fluctuations of the magnetization produce broadening of the resonance line. Now, the mean-square fluctuations of the magnetization can be expressed as:

$$\left\langle (\Delta M)^2 \right\rangle = \frac{T_C \chi}{V} \propto |T_C - T|^{-1}, \quad (2)$$

where χ is the magnetic susceptibility and V is the volume. So, the fluctuation of M is inversely proportional to the square root of the temperature deviation from the Curie point (T_C) [23]. In scaling theory, the exponent -1 is replaced by -1.4. The EPR line width ΔB, in turn, is proportional to the square root of the mean square fluctuations of the magnetization M, leading to Eq. (1).

4.2 Intense EPR Line at $g \sim 2.065$

The line at $g \sim 2.0$ does not exhibit significant temperature dependence. The line width can be fitted with a linear expression: $\Delta H(T) = \Delta H_0 + AT$, where $\Delta H = (890 \pm 20)$ G and $A = (-0.56 \pm 0.08)$ G/degree. It is proposed here that the Fe ions are in the superparamagnetic state, supported by the following arguments. (a) The g value is 2.065. (b) The temperature dependence of the double-

integrated intensity follows the Curie law within experimental error in the temperature region under study. (c) The double-integrated intensity, proportional to its magnetic moment, increases considerably with increasing pyrolysis temperature of the samples ($T > 1000$°C). (d) The content of the Fe ions in the samples remains the same; thus this increase can be only due to the formation of the nanostructure of SiCN ceramics with partly ordered Fe ions inside the nanograins of the ceramic.

5 Fourier-Transform Infrared (FTIR) and Raman Investigations of SiCN Ceramics

5.1 FTIR Investigations

A Perkin Elmer BX Spectrum FTIR spectrometer (MEMS laboratory, Department of Mechanical Engineering, Concordia University) was used for this study. The spectrum shown in Fig. 9 exhibits the presence of many IR (infrared) bands for the sample pyrolyzed at 600°C. The IR band at 2100 cm^{-1} is attributed to the Si–H chemical bond. This band disappears completely for the samples pyrolyzed at temperatures above 1000°C, as shown in Fig. 9, which exhibit only one broad band between 1250 cm^{-1} and 800 cm^{-1} due to Si–N and Si–C bonds. This is consistent with the FTIR spectra of SiCN derived from VNMS polymer [polymer with (ViSiHNMe)n silazane units; *Vi* vinyl, *Me* methyl] as described by Bahloul et al. [18]. No IR bands due to Si–Fe or C–Fe bonds were observed.

5.2 Raman Investigations

The spectra for various samples, as recorded using the Raman microspectrometer (Renishaw 3000 and Renishaw InVia) at University of Montreal, are shown in

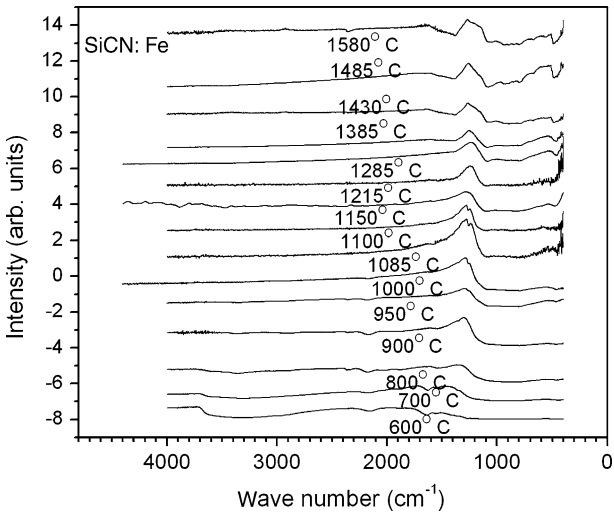

Fig. 9 Dependence of the FTIR spectra on the pyrolysis temperature of the samples

Fig. 10. They clearly reveal the successive transformations undergone by the carbon phase with pyrolysis temperature. Two low-intensity Raman bands, denoted as G and D, appear for the samples pyrolyzed at about 700°C due to the existence of the carbon phase in SiCN ceramic. They become intense for the samples pyrolyzed above 950°C. The D band corresponds to the amorphous state of carbon, whereas the less intense G band is due to the ordering of carbon atoms into graphene sheets [8, 10, 18, 24]. Two additional bands, D′ and G′, appear for the samples prepared at the pyrolysis temperature of 1400°C. In the samples prepared above the pyrolysis temperature of 1500°C, all Raman bands due to the free-carbon phase disappear, indicating their complete transformation into the SiCN ceramic network. The peculiar features of D′ and G′ bands are: (a) the D′ band (2,690 cm^{-1}) corresponds exactly to the second harmonic of the D band (1,350 cm^{-1}), unlike the G′ (2,930 cm^{-1}) band, and (b) there occurs splitting of the G band into two peaks (1580^{-1} and 1610 cm^{-1}) in the samples pyrolyzed at 1430 and 1485°C.

Characterization studies of the lattice disorder in carbon-based materials have shown that the second-order Raman spectra are often more sensitive to small variations of disorder in the crystal lattice than the first-order spectra [25]. The dominant feature in the second-order Raman spectra of carbon-based crystals is the appearance of a strong line at about 2,730 cm^{-1}, accompanied by a weak but sharp feature at about 3,250 cm^{-1}. The allowed lines in the Raman spectrum at 2,730 and 3,250 cm^{-1} correspond to the overtones of the maxima in the phonon density of states at about 1,350 and 1,610 cm^{-1}, respectively. A broad feature at about 2,970 cm^{-1} has been observed in the second-order spectrum of disordered carbon-materials, e.g., disordered graphite. This disorder-induced feature in the second-order Raman spectrum is not attributed to the second harmonic of G, rather it is associated with a combination mode from a high density of phonon states with different energies and different wave vectors: 1,350 cm^{-1} at the Brillouin zone

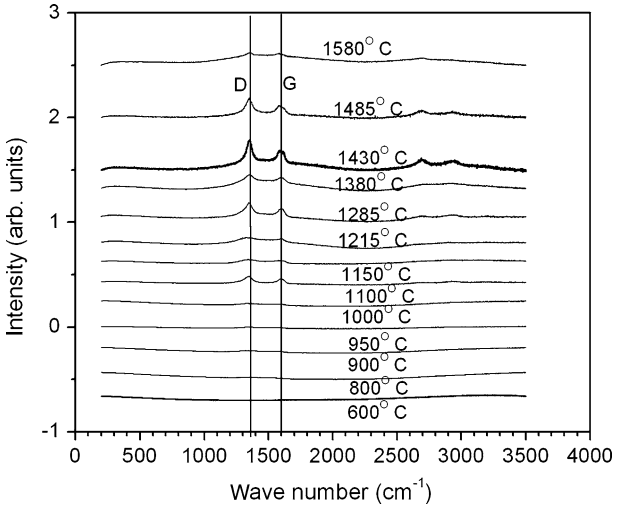

Fig. 10 Dependence of the Raman spectra on the pyrolysis temperature of the samples

boundary and 1,610 cm^{-1} in the mid-zone region. The mixing of modes with different wave vectors occurs through disorder or finite-size effects. The dominant disorder-induced Raman line in the first-order Raman spectrum occurs here at about 1,350 cm^{-1} and, in addition, a small disorder-induced feature appears at about 1,610 cm^{-1}. The positions of these bands depend on the pyrolysis temperatures of the samples. A splitting in frequency of the 1,580 cm^{-1} mode with decreasing pyrolysis temperature can be explained by the high density of phonon states away from the zone center. As the pyrolysis temperature is varied, distinct differences in the shape of the 1,580 cm^{-1} Raman band are observed.

6 X-ray Powder Diffraction Patterns

The X-ray powder patterns for the samples prepared at different pyrolysis temperatures are shown in Fig. 11. The changes in the X-ray patterns for various samples are in accordance with those for the pure SiCN ceramics [18] pyrolyzed at 1450°C, ascribed to β-Si_3N_4 clusters with hexagonal structure, as shown in Fig. 11. For the samples pyrolyzed at 1700°C, Li et al. [10] found the existence of only three peaks near $2\theta = 35°$. They ascribed these peaks to SiC crystallites. It implies that for the samples, pyrolyzed here above 1600°C, crystallization of SiC occurs. On the other hand, in the samples prepared at pyrolysis temperatures below 1500°C, crystallization of Si_3N_4 occurs. High-resolution X-ray patterns are shown in Fig. 12, where peaks from Fe_5Si_3 particles with hexagonal structure have been found [26]; however, not all peaks could be identified at present. A weak peak due to α-Fe particles was also observed here, similar to that reported by Saha et al. [13] for SiCN/Fe composites, where Fe incorporation was accomplished by the addition of the Fe_3O_4 powder. The X-ray diffraction peaks of crystalline graphite were also

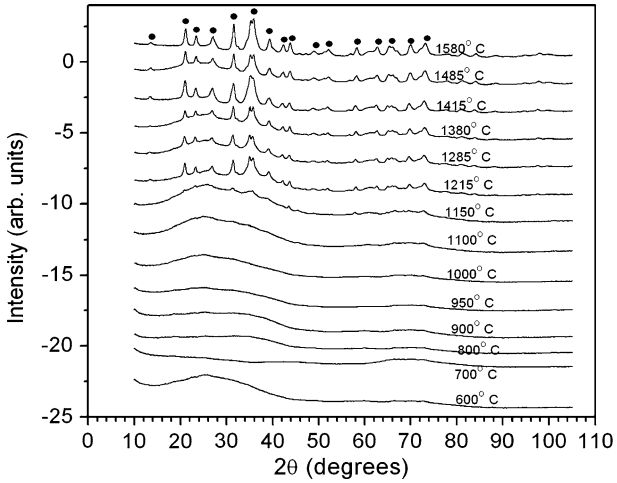

Fig. 11 Dependence of the X-ray patterns on the pyrolysis temperature of the samples. These *circles* marked on the peaks belonging to Si_3N_4 structure

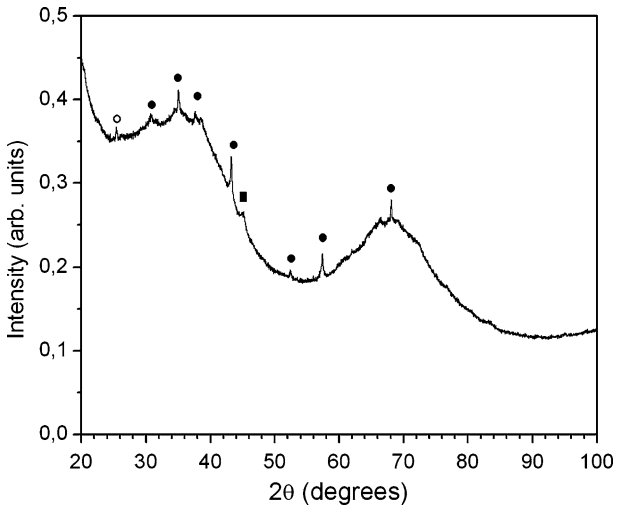

Fig. 12 X-ray diffraction pattern of the SiCN/Fe sample synthesized at 1100°C (increased sensitivity). The peak marked by *square* belongs to α-Fe. The peak marked by *open circle* belongs to graphite. The peaks marked by *circles* represent Fe_5Si_3 [26]

observed. High-resolution X-ray patterns of the SiCN sample pyrolyzed above 1300°C exhibit broadened X-ray diffraction peaks of Si_3N_4 together with additional peaks of iron-containing crystallites. The size of particles could be determined from broadening of X-ray diffraction. The size of the Si_3N_4 crystallites was estimated to be from 2 to 10 nm and it increased with pyrolysis temperature.

7 Magnetic Properties

SiCN ceramic samples were investigated at room temperature in a magnetic field of up to 2.2 T on a vibration sample magnetometer. As seen from Fig. 13, showing the magnetization versus the magnetic field, almost no hysteresis was found for all investigated samples. The coercive field decreases from about 15 for the SiCN/Fe samples prepared at 700°C to 1.0 mT for the samples prepared at 1200–1500°C. It corresponds to the soft ferromagnetic behavior of these samples. Ferromagnetism of nanoparticles with a rather large size (above 10 nm) suppresses here the superparamagnetism of Fe-containing nanoparticles with smaller dimensions. These data correspond to previously published data [20]. Temperature dependence of the magnetization at magnetic field of 1000 G was investigated in the range of 150–700 K and is shown in Fig. 14. From this dependence it is clearly seen that there are two different contributions to the magnetization: one from the ferromagnetic part of SiCN/Fe ceramics pyrolyzed at 1215°C with the phase-transition temperature of T_C = 400 K, and the second part from the superparamagnetic part of SiCN/Fe ceramics, following the Curie law. This Curie temperature (400 K) corresponds to that of Fe_5Si_3, and is supported by the EPR/FMR measurements. For the SiCN

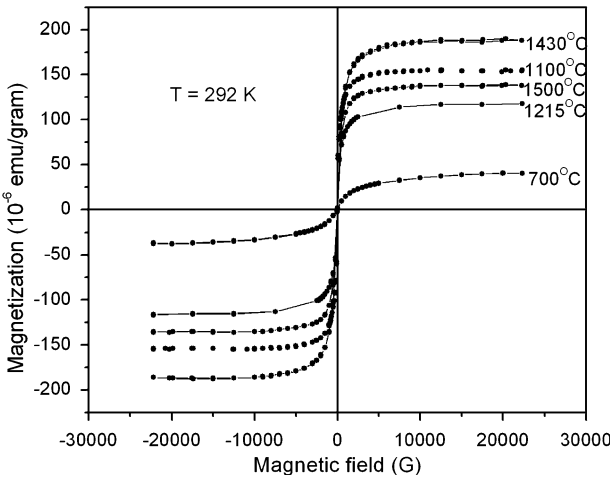

Fig. 13 Dependence of the magnetization on the magnetic field for SiCN/Fe samples pyrolyzed at different temperatures and measured at 292 K

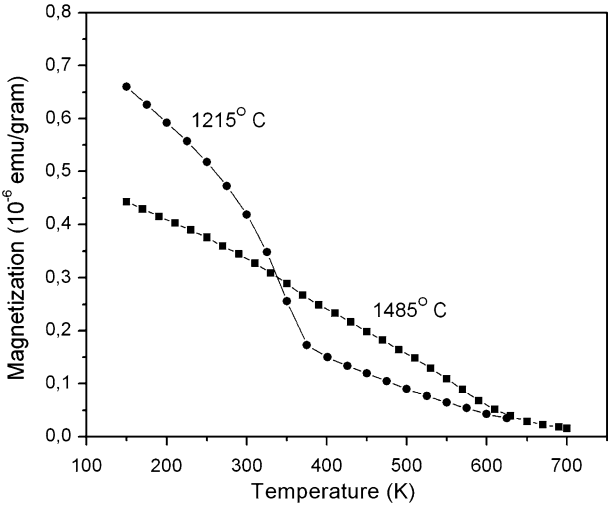

Fig. 14 Temperature dependence of the magnetization for SiCN/Fe samples pyrolyzed at different temperatures at 1,000 G

sample pyrolyzed at the higher temperature, 1485°C, the phase transition at 600 K was observed, which corresponds to a new ferromagnetic phase. Dependence of the saturation magnetization on the pyrolysis temperature is shown in Fig. 15. This dependence is similar to that of the double-integrated EPR intensity of the low-field line. This implies that the main part of the magnetization in SiCN/Fe ceramics is due to the nanoparticles of iron-containing crystallites, most likely those of Fe_5Si_3.

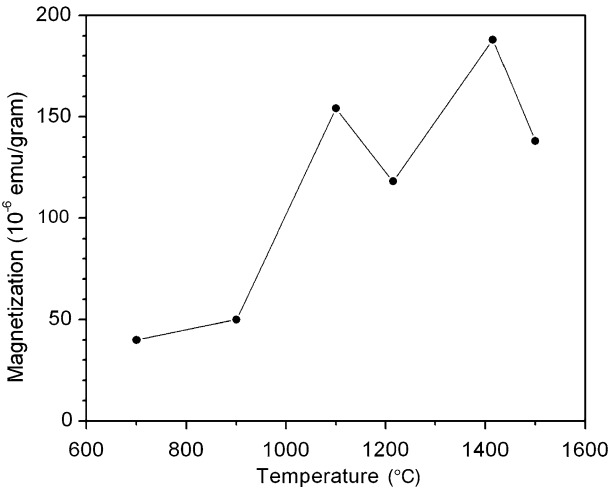

Fig. 15 Dependence of the saturation magnetization on the pyrolysis temperature measured at 292 K for various SiCN/Fe samples

8 Concluding Remarks

In this study, SiCN/Fe ceramic samples, synthesized at different pyrolysis temperatures in the range of 600–1580°C, were investigated by EPR/FMR. These samples consist of nanoparticles, significantly influencing the spectra. This is further supported by the data obtained here by X-ray diffraction, Raman and FTIR techniques. Three different states of Fe^{3+} ions were found in these samples: (a) Fe^{3+} ions incorporated into the free-carbon structure, characterized by superparamagnetic behavior exhibiting an enhanced magnetic moment. This signal is further split into two, those due to the ordered and the amorphous free-carbon phases. It is characterized by transformation from the paramagnetic state for the samples pyrolyzed at temperature of 600–800°C to the superparamagnetic state for the samples synthesized at temperature of 950–1150°C. (b) Fe_5Si_3 particles characterized by ferromagnetic behavior. The signal corresponding to this phase appears in the samples pyrolyzed at 950°C and disappears in the samples pyrolyzed at 1400°C. (c) The third type of Fe^{3+} ions exhibit the narrow line near $g = 2.0$ manifested only in the samples synthesized above 1200°C. They are probably incorporated into the Si–C–N nano-crystallites. These signals disappear in the samples pyrolyzed above 1530°C.

The studies reported here using the techniques of EPR/FMR X-ray, Raman, and magnetic measurements provide sufficient information on the characteristics of the SiCN/Fe samples, so that they can be exploited for MEMS applications.

Acknowledgments We are grateful to Dr. T. Maris from Montreal University for recording X-ray patterns, Dr. S. Elouatik from Montreal University for recording Raman spectra and helpful discussions, and Dr. G. Kennedy from the SLOWPOKE Reactor laboratory of Ecole Polytecnique for neutron activation analysis of these samples. S.A. and I.S. are grateful for support from Consortium de Recherché et d' Innovation en Aerospatiale au Quebec (CRIAQ) and Pratt and Whitney, Canada. S.K.M. is grateful

for partial financial support from the Natural Sciences and Engineering Research Council (NSERC) of Canada.

References

1. V.M. Bright, R. Raj, M.L. Dunn, J.W. Daily, Injectable ceramic microcast silicon carbonitride (SiCN) microelectromechanical system (MEMS) for extreme temperature environments with extension: micro packages for nano-devices, Colorado University, AFRL-IF-RS-TR-2004, Final Technical Report
2. L.-A. Liew, R.A. Saravanan, V.M. Bright, M.L. Dunn, J.W. Daily, R. Raj, Sens. Actuators A **103**(1–2), 171–181 (2003)
3. H. Fujimori, S. Ohnuma, N. Kobayashi, T. Masumoto, J. Magn. Magn. Mater. **304**(1), 32–35 (2006)
4. J. Bill, T.W. Kamphowe, A. Muller, T. Wichmann, A. Zern, A. Jalowieki, J. Mayer, M. Weinmann, J. Schuhmacher, K. Muller, J.Q. Peng, H.J. Seifert, F. Aldinger, Appl. Organomet. Chem. **15**(10), 777–793 (2001)
5. A. Saha, R. Raj, D.L. Williamson, H.-J. Kleebe, J. Am. Ceram. Soc. **88**(1), 232–234 (2005)
6. S.I. Andronenko, I. Stiharu, S.K. Misra, J. Appl. Phys. **99**, 113907(1–5) (2006)
7. S. Trassl, G. Motz, E. Rossler, G. Ziegler, J. Non-Cryst. Solids **293–295**, 261–267 (2001)
8. S. Trassl, G. Motz, E. Rossler, G. Ziegler, J. Am. Ceram. Soc. **85**(1), 239–244 (2002)
9. S. Trassl, H.-J. Kleebe, H. Stormer, G. Motz, E. Rossler, G. Ziegler, J. Am. Ceram. Soc. **85**(5), 1268–1274 (2002)
10. Y.-L. Li, E. Kroke, R. Riedel, C. Fasel, C. Gervais, F. Babonneau, Appl. Organometal. Chem. **15**(11), 820–832 (2001)
11. A. Saha, R. Raj, D.L. Williamson, J. Am. Ceram. Soc. **89**(7), 2188–2195 (2006)
12. A. Saha, R. Raj, J. Am. Ceram. Soc. **90**(2), 578–583 (2007)
13. A. Saha, S.R. Shah, R. Raj, S.E. Russek, J. Mater. Res. **18**(11), 2549–2551 (2003)
14. A. Dumitru, V. Ciupina, I. Stamatin, G. Prodan, A. Morozan, C. Mirea, J. Optoelectron. Adv. Mater. **8**(1), 50–54 (2006)
15. A. Dumitru, I. Stamatin, A. Morozan, C. Mirea, V. Ciupina, Mater. Sci. Eng. C **27**(5–8), 1331–1337 (2007)
16. Y. Li, Z. Zheng, C. Reng, Z. Zhang, W. Gao, S. Yang, Z. Xie, Appl. Organometal. Chem. **17**(2), 120–126 (2003)
17. J. Li, Z. Zhang, Z. Zheng, L. Guo, G. Xu, Z. Xie, J. Appl. Polym. Sci. **105**(4), 1786–1792 (2007)
18. D. Bahloul, M. Pereira, C. Gerardin, J. Mater. Chem. **7**(1), 109–116 (1997)
19. C. Gerardin, F. Taulelle, D. Bahloul, J. Mater. Chem. **7**(1), 117–126 (1997)
20. M.J. MacLachlan, M. Ginzburg, N. Coombs, T.W. Coyle, N.P. Raju, J.E. Greedan, G.A. Ozin, I. Manners, Science **287**(5457), 1460–1463 (2000)
21. T.S. Altshuler, M.S. Bresler, Yu. V. Goryunov, JETP Lett. **81**(9), 475–478 (2005)
22. E. Sawatzky, IEEE Trans. Magn. **7**(3), 374–376 (1971)
23. L.D. Landau, E.M. Lifshitz, in Course of Theoretical Physics, vol. 5: Statistical Physics, 4th edn. (Nauka, Moscow, 1995; Butterworth, London, 1999), p. 528
24. F. Tuinstra, J.L. Koenig, J. Chem. Phys. **53**(3), 1126–1130 (1970)
25. R.O. Dillon, J.A. Woollam, V. Katkanant, Phys. Rev. B. **29**(6), 3482–3489 (1984)
26. M. Mukaida, I. Hiyama, T. Tsunoda, Y. Imai, in Proceedings of 17th International Conference on Thermoelectrics, IST 98, 237–240 (1998), p. 542